Proceedings of the
Annual Stability Conference
Structural Stability Research Council
Nashville, Tennessee, March 24-27, 2015

OpenSees simulation of steel column axial cyclic response including local buckling

David A. Padilla-Llano[1], Cristopher D. Moen[2], Matthew R. Eatherton[3]

Abstract
This paper presents an approach for simulating steel column axial cyclic response including local buckling deformation. Two methods are proposed – (1) a *nonlinear spring* model with concentrated nonlinear *axial load-displacement* (*P-δ*) behavior, and (2) a *nonlinear beam-column* model with distributed nonlinear section *axial load-strain* (*P-ε*) behavior. The models are implemented in OpenSees using *Pinching4* as the underlying behavior model with parameters derived as a function of the dissipated energy, and cross-sectional slenderness λ_ℓ. Parameter relationships are informed by recent lipped C-section cold-formed steel cyclic experiments and finite element simulations. The proposed methodology is established for thin-walled cold-formed steel members, however the *Pinching4* parameters are posed generally as a function of local buckling slenderness and could be extended to hot-rolled steel members and cross-sections with future validation.

1. Introduction

Steel columns subjected to dynamic loading such as those resulting from earthquakes wind, and others, can experience local buckling deformations that reduce their strength and affect their ductility. Local buckling deformations develop under compression and stretch during tension, and this effect is more pronounced in thinner cross-sections (e.g., thin-walled cold-formed steel). During cyclic loading, buckling deformations reverse and combine with yielding in tension at the highly stressed locations compromising the member's strength and stiffness.

The axial cyclic responses obtained by Padilla-Llano et al. (2014a) for cold-formed steel studs under cyclic axial load showed how local buckling affected the *P-δ* response and influenced directly where damage and fracture occurred in the member. Fig. 1 shows that strength and stiffness started deteriorating as soon as considerable local web buckling deformations developed (at the peak compressive load). Additionally, the rate of energy dissipation increases after the peak compression load through yielding by folding and stretching of the buckled web. Results from finite element simulations of plates subjected to cyclic loading (previously performed by the authors) demonstrated that energy dissipation and damage accumulates in zones that correspond

[1] Graduate Research Assistant, Civil & Environmental Engineering, Virginia Tech, <dapadill@vt.edu>
[2] Associate Professor, Civil & Environmental Engineering, Virginia Tech, <cmoen@vt.edu>
[3] Assistant Professor, Civil & Environmental Engineering, Virginia Tech,<meather@vt.edu>

to the leading buckled half-waves i.e., the half-waves with bigger deformation (Padilla-Llano et al. 2014b). Damage localizes in these zones once inelastic strains starts to accumulate until they lead failure/fracture around one of these zones at the late stages of the response (see Fig. 2).

This paper presents a computationally efficient approach to model the axial cyclic response of steel columns including local buckling. The approach is supported by the experimental and finite element analysis results concerning local buckling effects in the thin-walled member axial cyclic response presented previously by the authors (Padilla-Llano et al. 2014a,b). The modeling approach introduced uses *Pinching4* as the format for the underlying behavior model and is implemented in OpenSees (Lowes 2004, Mazzoni 2009). Generalized expressions for backbones, strength degradation, stiffness degradation and pinching parameters are presented as a function of the member cross-section slenderness and the hysteretic energy dissipated. The model parameters are derived using *P-δ* responses obtained from finite element analysis of thin-walled cold-formed steel members conducted in ABAQUS (2013).

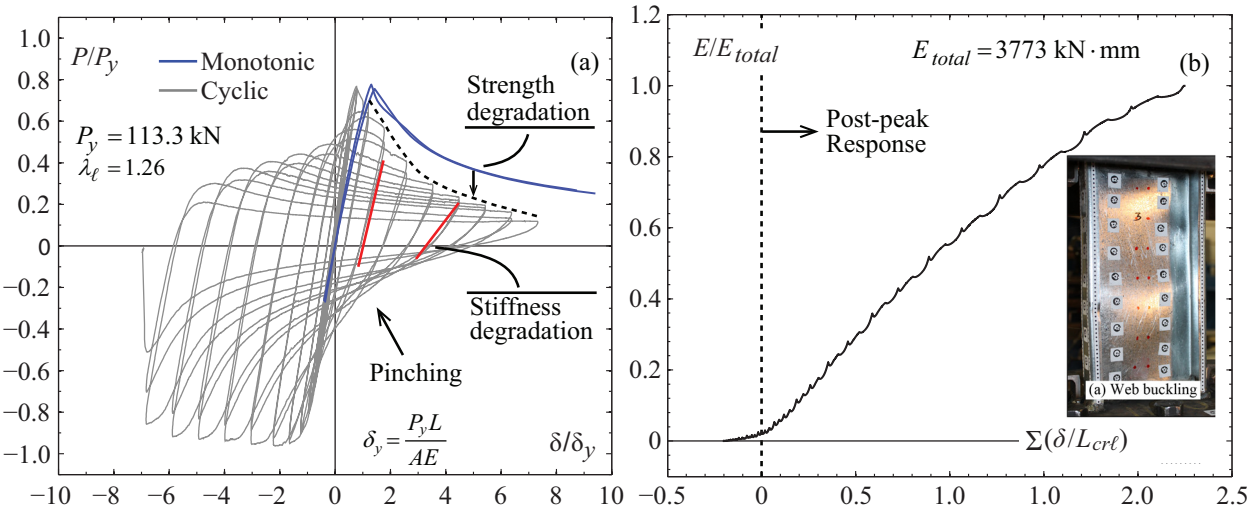

Figure 1: The cyclic axial response *P-δ* (a) shows strength and stiffness degradation due to local buckling deformations (b) in the member. Energy dissipation occurs through yielding of the buckled web.

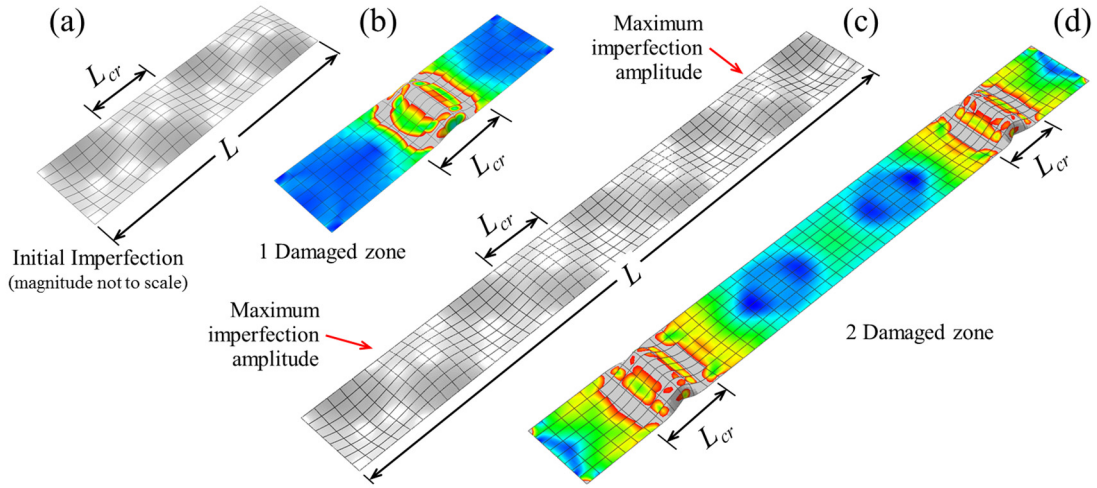

Figure 2: Damage due to cyclic loading accumulates in zones corresponding to the leading half-wave (a, b) or areas with bigger initial imperfections (c, d). Damage does not propagate to other areas once it starts at these locations.

2. Axial Hysteretic Modeling of Steel Columns Including Local Buckling

Two approaches to model the axial cyclic load-deformation response of thin-walled members experiencing local-buckling are discussed next. The first approach considers *nonlinear springs* to capture the member *axial load-displacement* (*P-δ*) response. The second approach consist of a *nonlinear beam-column* element with distributed nonlinear *axial load-strain* (*P-ε*) section behavior capable of capturing the member load-deformation response. Fig. 1 demonstrates both approaches for an axial member subjected to uniform axial loading. The underlying behavior model used in both introduced approaches is shown in Fig. 1d and consists of a *backbone curve*, *unloading-reloading paths* that account for pinching, and a *damage model* for strength and stiffness degradation. This formulation is based on the material model *Pinching4* as implemented in OpenSees (Lowes 2004, Mazzoni 2009).

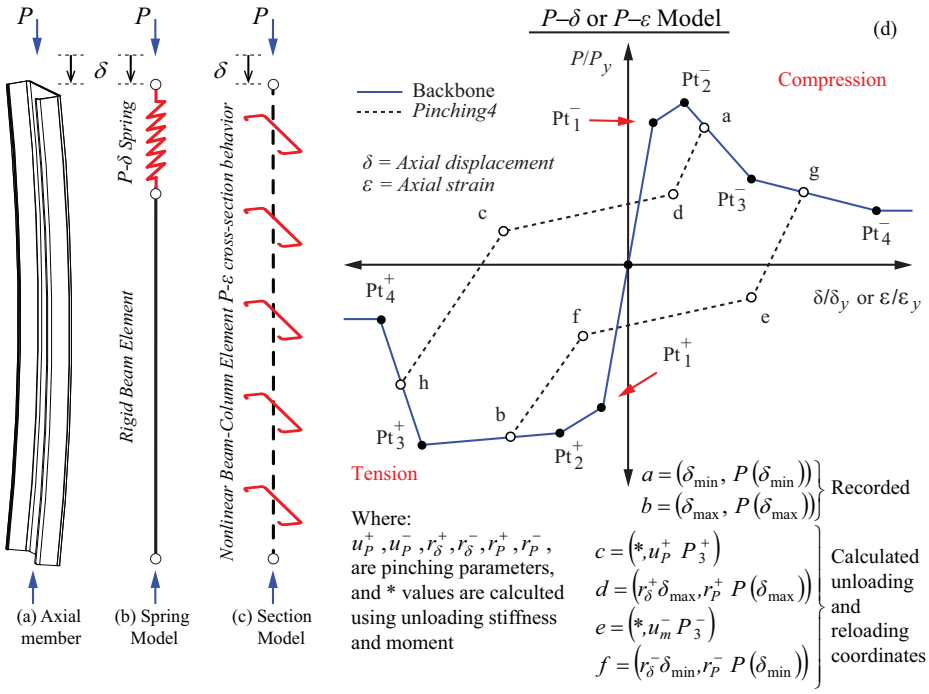

Figure 3: Axial hysteretic models for thin-walled steel axial members subjected to uniform axial load and experiencing local buckling

2.1. Spring Model - Concentrated Nonlinearity

The spring model uses rigid beam elements connected to *nonlinear springs* where all the nonlinear behavior concentrates. These springs are located at preselected locations along the modeled member length and their number and distribution would depend on the loading conditions. Fig. 1b illustrates how a thin-walled steel member subjected to uniform axial loading can be modeled using a spring at the top end to capture the axial cyclic load-deformation response. For axial loads varying along the member length, additional springs should be located strategically such that the member response is accurately modeled. Using nonlinear springs is a computationally inexpensive approach but requires adjusting the hysteretic material model parameters depending on possible different member lengths and loading conditions.

2.2. Nonlinear Beam-Column Model - Distributed Nonlinearity

The *nonlinear beam-column element* model with distributed nonlinearity is implemented using an *axial load-strain P-ε* formulation to model the response at the cross-section level (Fig. 1c). The parameters to define the cross-section *P-ε* behavior are derived from the corresponding values defining the nonlinear spring model previously described. The strains coordinates in the backbone *P-ε* for thin-walled axial members subjected to uniform axial loading are obtained by dividing the axial displacement δ_i by the member length L, thus $\varepsilon_i = \delta_i / L$. Parameters to model strength degradation, stiffness degradation and pinching are the same defined for the nonlinear spring model. The distributed nonlinearity approach allows flexible modeling of thin-walled steel members subjected to different axial loading conditions (e.g. non-uniform axial load) using the same set of parameters for all cross-sections in the beam-column element.

The authors have previously shown how the two modeling approaches are capable of capturing the axial cyclic response of tested cold-formed steel members (Padilla-Llano et al. 2014b). Next, the just cited work is extended for thin-walled steel members where the parameters defining the spring and cross-section behavior in Fig. 1d are formulated for any local cross-section slenderness.

3. Finite Element Analysis Database for Hysteretic Model Calibration

Parameters for the underlying hysteretic model that define the spring and beam-column behavior are obtained through direct calibration of *Pinching4* to match simulated axial load-displacement (*P-δ*) monotonic and cyclic responses of thin-walled members. A set of twenty two thin-walled C-shaped columns were modeled using ABAQUS (2013) to study the monotonic and cyclic behavior of axial members exhibiting local buckling deformations. The cross-sections were selected from the Structural Stud Manufacturers Association catalog (SSMA 2011) covering a range of local cross-section slenderness $\lambda_\ell = (P_y / P_{cr\ell})^{0.5}$ from 0.69 to 3.39 ($P_y = AF_y$, A=cross-section area; F_y=yield stress). The capacity in compression for all modeled columns as predicted by the American Iron and Steel Institute (AISI) Direct Strength Method (AISI 2007) is governed by local buckling.

The models are implemented using S9R5 thin-shell elements and member length was set such that at least five buckling half-waves could develop in compression. The geometry and boundary conditions are illustrated in Fig. 2a. Initial geometric imperfections are simulated using the 1D spectral approach described by Zeinoddini et al. (2012). The modulus of elasticity is assumed as E=203.4GPa and Poisson's ratio ν=0.3. Steel plasticity is implemented using combined isotropic-kinematic hardening with one backstress with the parameters summarized in Fig. 2c. Material damage is also simulated to capture the strength and stiffness reduction from tearing and fracture caused by cold-bending and stretching during cyclic loading.

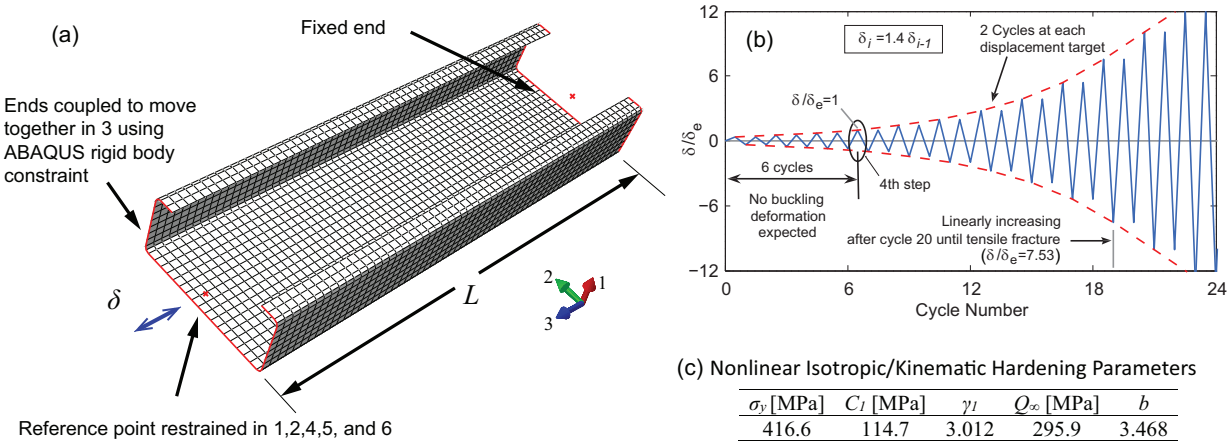

(c) Nonlinear Isotropic/Kinematic Hardening Parameters

σ_y [MPa]	C_1 [MPa]	γ_1	Q_∞ [MPa]	b
416.6	114.7	3.012	295.9	3.468

Figure 4: Finite element model geometry (a), displacement-controlled loading protocol (b), and steel material hardening parameters (c)

The members are loaded at one end by imposing a displacement history using the displacement-controlled testing protocol for cold-formed steel members introduced by Padilla-Llano et al. (2014a). This protocol is symmetric with steps of increasing amplitude and two cycles per step. Each step's amplitude is 40% larger than the previous (i.e., δ_i=1.4δ_{i-1}), see Fig. 2b. The protocol is anchored at the fourth step to the elastic displacement $\delta_e=(0.776)^2 P_{cr\ell} L/AE$ where $P_{cr\ell}$ is the elastic local buckling load. The finite element analysis protocol was validated against the experimental cyclic responses of cold-formed steel studs experiencing local buckling deformations obtained by Padilla-Llano et al. (2014a), see Fig. 3.

Each model in the column set was analyzed to obtain axial load-displacement (P-δ) monotonic and cyclic responses. This set of responses were characterized to obtain the amount of strength degradation, stiffness degradation, hysteretic energy dissipated and pinching. The procedures to characterize the load-displacement P-δ response are described elsewhere (Padilla-Llano et al. 2013a,b).

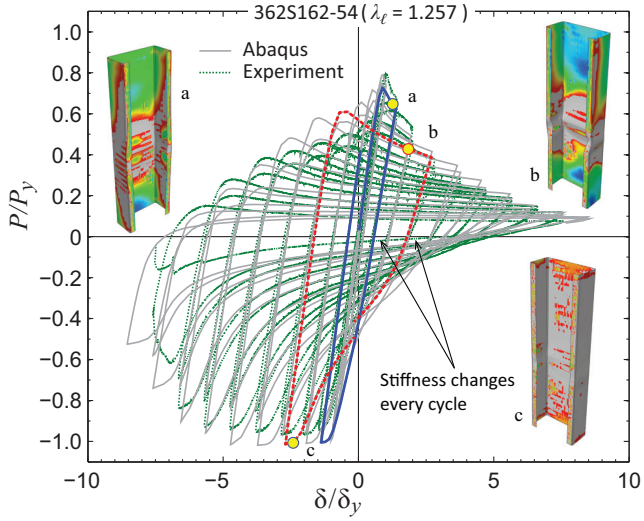

Figure 5: Experimental and simulated cyclic responses are compared to validate the finite element analysis protocol.

4. Hysteretic Model for Members Including Local Buckling

The monotonic and cyclic axial displacement (P-δ) responses for each of the 22 models were used to obtain backbone curves and calibrate parameters for strength degradation, stiffness degradation and pinching compatible with the *Pinching4* model. General expressions were then derived for each parameter as a function of the cross-section local slenderness λ_ℓ, the yield load P_y and the corresponding elastic yield displacement $\delta_y=P_yL/AE$ (or strain $\varepsilon_y=\delta_y/L$). The resulting generalized expressions are described next.

4.1. Backbone Curve

Expressions for the four coordinate pairs (δ_i, P_i) [or (ε_i, P_i)] that define the backbone curve in compression are summarized in Table 1 and illustrated in Fig. 4a. The load values P_i are set as a function of the local slenderness λ_ℓ where the peak load P_2 is set equal to the DSM strength expression in AISI-S100-07 (AISI 2007). All values of P_i are limited to a maximum of P_y with the case where all $P_i/P_y = 1.0$ corresponding to a column with a very stocky cross-section (i.e. compact cross-section). To determine the displacement δ_1 (strain ε_1) that marks the end of the elastic range in compression, it is necessary to calculate the initial stiffness k_1 expressed as a fraction (that depends on λ_ℓ) of the elastic stiffness $k_e=AE/L$ (see Fig. 5). The expressions for the initial stiffness k_1 and the compressive load P_1 suggests that the cross-section is considered fully effective for $\lambda_\ell \leq 0.689$, and considered slender if $\lambda_\ell > 1.23$. The remaining δ_i (ε_i) values are calculated as indicated in Table 1.

The tension backbone coordinate pairs (δ_i, P_i) [or (ε_i, P_i)] are set as a function of the yield load P_y and the corresponding elastic yield displacement δ_y (or strain ε_y). One of the shortcomings of the *Pinching4* hysteretic model as currently implemented is that while the backbone can be separately defined in compression and tension, the strength and stiffness degradation parameters are universal to both loading directions (see section 5.2). However, the effect of the accumulation of damage in compression compare to tension is significantly different as shown by the finite element analysis and the experimental work conducted by the authors (Padilla-Llano et al. 2014a). Therefore, a tension backbone was developed with load values P_i slightly larger than P_y, such that the overall simulated response match best the responses from ABAQUS. The tension backbone coordinates are listed in Table 2.

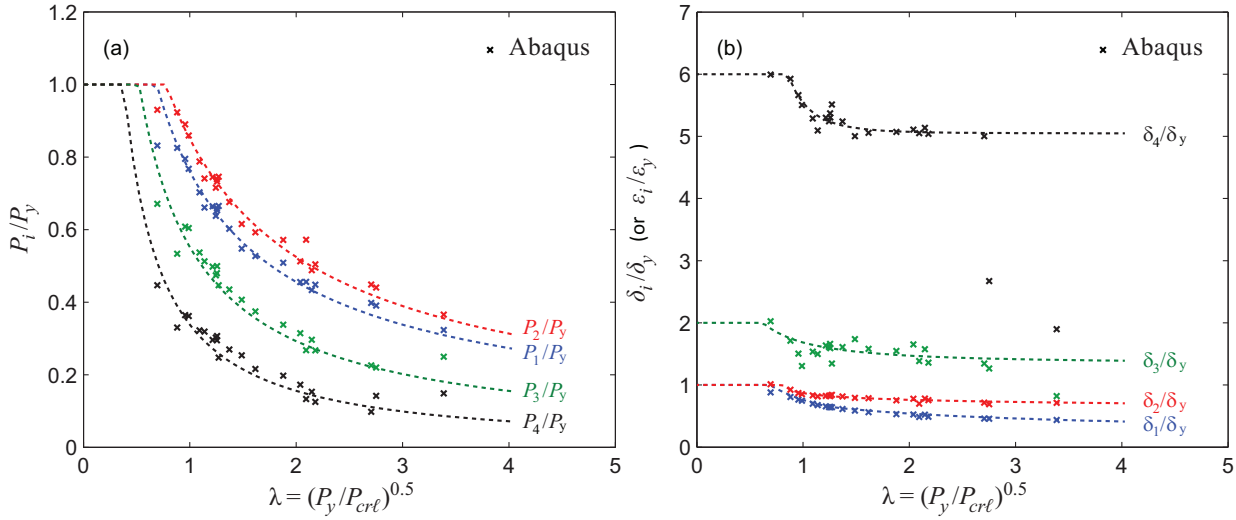

Figure 6: Compression backbone general expressions for local buckling

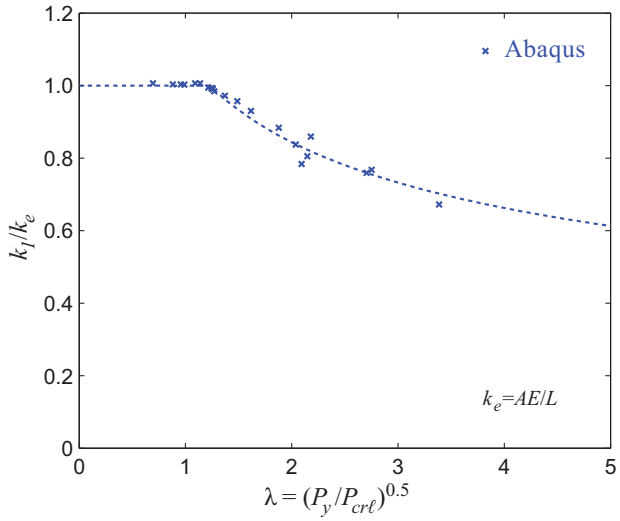

Figure 7: Initial member stiffness as a function of local slenderness.

Table 1: Compression backbone general expressions for local buckling

Load	Displacement/Strain
$\frac{P_1}{P_y} = \begin{cases} 1.0 & ,\lambda_\ell \le 0.689 \\ 0.760\lambda_\ell^{-0.737} & ,\lambda_\ell > 0.689 \end{cases}$	$\frac{\delta_1}{\delta_y} = \frac{\varepsilon_1}{\varepsilon_y} = \begin{cases} 1.0 & ,\lambda_\ell \le 0.689 \\ P_1/k_1 & ,\lambda_\ell > 0.689 \end{cases}$
$\frac{P_2}{P_y} = \begin{cases} 1.0 & ,\lambda_\ell \le 0.776 \\ \left[1-0.15\lambda_\ell^{-2(0.4)}\right]\lambda_\ell^{-2(0.4)} & ,\lambda_\ell > 0.776 \end{cases}$	$\frac{\delta_2}{\delta_y} = \frac{\varepsilon_2}{\varepsilon_y} = \begin{cases} 1.0 & ,\lambda_\ell \le 0.814 \\ 0.774\left(\lambda_\ell - 0.776\right)^{-0.078} & ,\lambda_\ell > 0.814 \end{cases}$
$\frac{P_3}{P_y} = \begin{cases} 1.0 & ,\lambda_\ell \le 0.523 \\ 0.552\lambda_\ell^{-0.915} & ,\lambda_\ell > 0.523 \end{cases}$	$\frac{\delta_3}{\delta_y} = \frac{\varepsilon_3}{\varepsilon_y} = \begin{cases} 2.0 & ,\lambda_\ell \le 0.623 \\ 1.339 + 0.345\lambda_\ell^{-1.371} & ,\lambda_\ell > 0.623 \end{cases}$
$\frac{P_4}{P_y} = \begin{cases} 1.0 & ,\lambda_\ell \le 0.379 \\ 0.338\lambda_\ell^{-1.119} & ,\lambda_\ell > 0.379 \end{cases}$	$\frac{\delta_4}{\delta_y} = \frac{\varepsilon_4}{\varepsilon_y} = \begin{cases} 6.0 & ,\lambda_\ell \le 0.857 \\ 5.048 + 0.491\lambda_\ell^{-4.287} & ,\lambda_\ell > 0.857 \end{cases}$
	$\frac{k_1}{k_e} = \begin{cases} 1.0 & ,\lambda_\ell \le 1.23 \\ 1.075\lambda_\ell^{-0.349} & ,\lambda_\ell > 1.23 \end{cases}$

Table 2: Tension backbone general expressions for local buckling

Load	Displacement/Strain
$P_1/P_y = 1.044$	$\delta_1/\delta_y = \varepsilon_1/\varepsilon_y = 1.044$
$P_2/P_y = 1.134$	$\delta_2/\delta_y = \varepsilon_2/\varepsilon_y = 1.404$
$P_3/P_y = 1.172$	$\delta_3/\delta_y = \varepsilon_3/\varepsilon_y = 8.0$
$P_4/P_y = 0.872$	$\delta_4/\delta_y = \varepsilon_4/\varepsilon_y = 10.0$

4.2. Cyclic Strength Degradation

Cyclic strength degradation is simulated as a function of the *cumulative hysteretic energy dissipated* in each excursion E_i and the *total energy dissipation capacity* E_T (see section 5.5). As more hysteretic energy is dissipated, the ratio E_i/E_T approaches unity where further deterioration is not expected. The functional form for strength degradation is shown in Table 3 where the

coefficients $\beta_{2,s}$ and $\beta_{4,s}$ are calibrated using the responses from the finite element analysis database.

Strength degradation is characterized as the positive difference on strength between the monotonic backbone force ($f_{max,o}$) and the cyclic force envelope ($f_{max,i}$). Strength degradation differs substantially between compression and tension excursions as shown in Fig. 6a. In *Pinching4*, deterioration of the strength envelope is defined using the same set of parameters for tension and compression. Further, the damage accumulated during compression excursions is used to reduce the strength envelope for the subsequent excursions in tension (and vice versa). If damage accumulated from previous excursion is used in the current (but opposite in direction) excursion, then strength degradation will be slightly underestimated and overestimated during the compression and tension excursions respectively. This shortcoming was addressed herein by setting the loads P_i for the tension backbone slightly larger than P_y (see section 5.1) while setting parameters $\beta_{2,s}$ and $\beta_{4,s}$ equal for both loading directions. $\beta_{2,s}$ and $\beta_{4,s}$ are derived using the average strength degradation in tension and compression for each member.

Because strength degradation is member length and cross-section slenderness independent in both tension and compression (see Fig. 6a), parameters $\beta_{2,s}$ and $\beta_{4,s}$ are set constant (see Table 3). Note also that there is some residual strength after the energy dissipation capacity is exhausted (i.e., E_i/E_T =1.0).

4.3. Cyclic Stiffness Degradation

Cyclic stiffness degradation is also defined as a function of the *cumulative hysteretic energy dissipated* in each excursion E_i and the *total energy dissipation capacity* E_T (see section 5.5). As in the case of strength degradation, when E_i/E_T =1.0 further decrease in stiffness is not expected. Stiffness degrades as indicated in Table 3, where the coefficients $\beta_{2,k}$ and $\beta_{4,k}$ are calibrated using the responses from the finite element analysis database.

Stiffness degradation is characterized as the difference between the member initial stiffness k_1 and the unloading stiffness in every excursion k_i where unloading stiffness values are obtained as described by Padilla-Llano et al. (2013a,b). The differences between unloading stiffness degradation in tension and compression are even greater than the differences in strength degradation as shown in Fig. 6b. In addition, the figure shows that stiffness degradation in compression is more pronounced for more slender members (indicated by the lighter colors), while in tension degradation is independent of the member length and cross-section slenderness. Stiffness appears to reduce to zero as the cumulative energy dissipated E_i reaches the maximum value E_T.

As in the case of strength degradation, deterioration of the stiffness is defined using the same set of parameters for tension and compression using the current implementation of the *Pinching4* model. Thus, the damage accumulated during compression excursions is used to reduce the stiffness for the subsequent excursions in tension (and vice versa). Overestimated and underestimated stiffness in compression and tension excursions respectively is expected if the same set of parameters $\beta_{2,k}$ and $\beta_{4,k}$ is used in both loading directions. No steps were taken to address this shortcoming as the initial stiffness k_1 should not be modified. The resulting expression

for stiffness degradation parameters $\beta_{2,s}$ and β_4 as a function of the cross-section slenderness λ_ℓ are summarized in Table 3 and illustrated in Fig. 7.

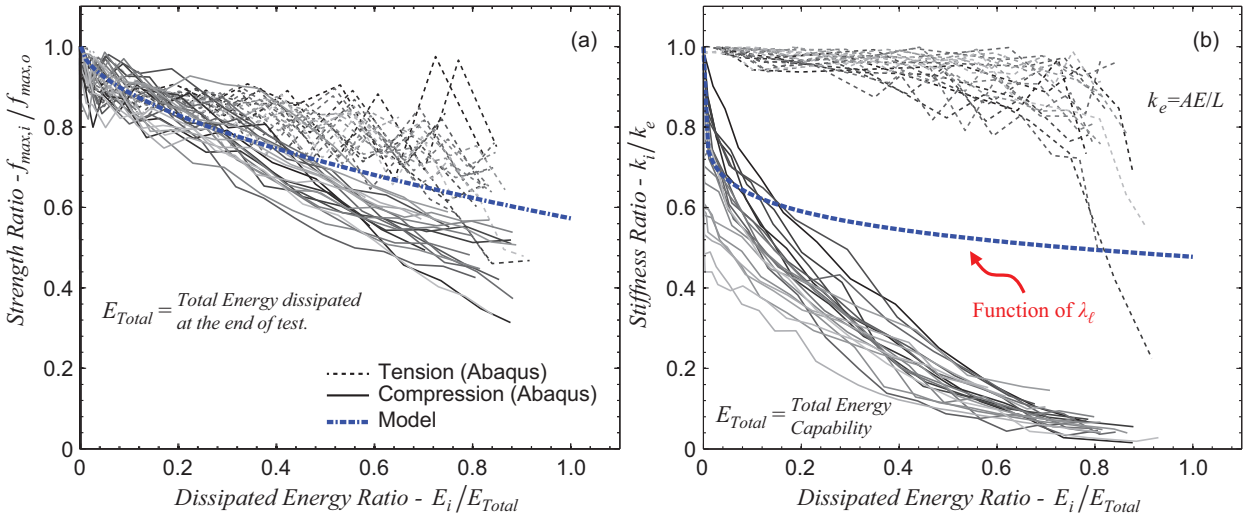

Figure 8: Strength degradation (a) is independent of the member length and cross-section slenderness, while stiffness degradation (b) is a function of the member cross-section slenderness. Both strength and stiffness degradation are expressed as a function of the hysteretic energy dissipated.

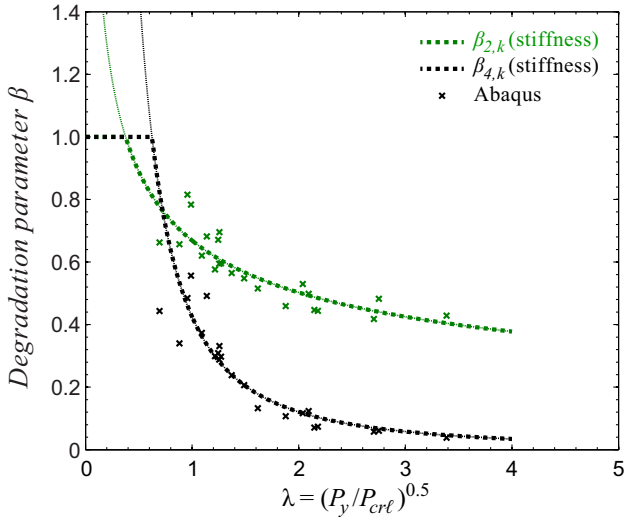

Figure 9: Stiffness degradation parameters as a function of the cross-section slenderness

Table 3: Strength and stiffness degradation parameters

Strength Degradation	Stiffness Degradation
$f_{\max,i}/f_{\max,o} = 1-\beta_{2,s}\left(E_i/E_T\right)^{\beta_{4,s}} \le 1.0$	$k_i/k_1 = 1-\beta_{2,k}\left(E_i/E_T\right)^{\beta_{4,k}} \le 1.0$
$\beta_{2,s} = 0.427$	$\beta_{2,s} = \begin{cases} 1.0 & ,\lambda_\ell \le 0.377 \\ 0.669\lambda_\ell^{-0.412} & ,\lambda_\ell > 0.377 \end{cases}$
$\beta_{4,s} = 0.569$	$\beta_{4,s} = \begin{cases} 1.0 & ,\lambda_\ell \le 0.624 \\ 0.425\lambda_\ell^{-1.814} & ,\lambda_\ell > 0.624 \end{cases}$

4.4. Unloading-Reloading Behavior (Pinching)

The unloading-reloading behavior is defined by six parameters, u_{P+}, u_{P-}, $r_{\delta+}$, $r_{\delta-}$, r_{P+} and r_{P-}. The parameters $r_{\delta-}$ and $r_{\delta+}$ are the ratio of the deformation at which reloading starts (points *d* and *f* in Fig. 2d) to the maximum/minimum historic deformation, d_{min} and d_{max}. Parameters r_{P-} and r_{P+} are the corresponding ratios of the load at the point at which reloading starts (points *d* and *f*) to the load corresponding to the maximum historic displacement, $f(d_{min})$ and $f(d_{max})$. Parameters u_{P-} and u_{P+} are the ratios of the load developed after unloading (point *c* and *e* in Fig. 1d) to the load coordinate of backbone point 3, P_{3-} and P_{3+}.

The unloading-reloading parameters were obtained as described by Padilla-Llano et al. (2013a,b) for each of the responses in the finite element database and are shown in Fig. 8. The figure shows that the pinching parameters are similar for all members analyzed and therefore and average value for u_{P+}, u_{P-}, $r_{\delta+}$, $r_{\delta-}$, r_{P+} and r_{P-} was adopted (see Table 4).

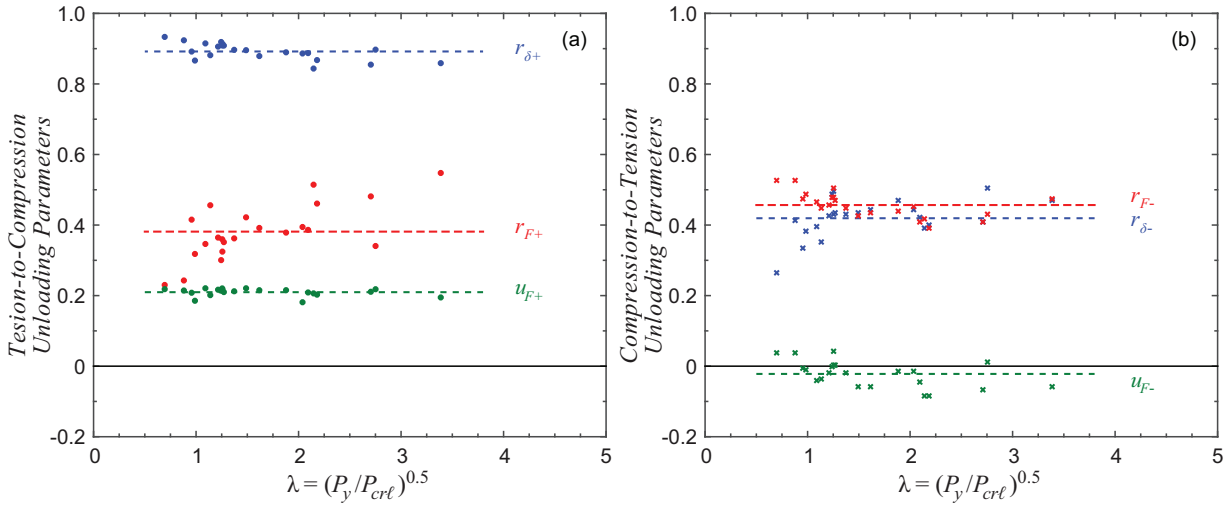

Figure 10: Unloading-reloading path parameters for (a) tension-to-compression and (b) compression-to-tension

Table 4: Unloading-reloading path parameters

Parameter	$r_{\delta+}$	r_{P+}	u_{P+}	$r_{\delta-}$	r_{P-}	u_{P-}
Mean	0.381	0.892	0.210	0.419	0.457	-0.022
COV	0.207	0.026	0.052	0.130	0.081	-1.702

4.5. Total Energy E_T

It was shown previously that stiffness and strength degrade as a function of the *cumulative hysteretic energy dissipated* in each excursion E_i and the *total energy dissipation capacity* E_T. The total energy dissipation capacity E_T is the maximum value of cumulative hysteretic energy the element is allow to dissipate. A general expression to calculate E_T for any given member represents a challenge as this value cannot be tide easily to the member strength and properties in a mechanics based manner. However, a heuristic procedure based on the hysteretic energy dissipated per excursion was developed to obtain an expression for E_T given the member cross-section slenderness λ_ℓ.

The procedure to obtain E_T starts by calculating the *hysteretic energy dissipated* per excursion $E_{e,i}$ normalized to an area defined by the maximum load in the corresponding loading direction and

the range of deformations of the current excursion (see inset in Fig. 9a). If this normalized energy dissipated per excursion ($NHE_{pe,i}$) is plotted versus the cumulative normalized axial deformation ($\sum\delta/\delta_y$), the plot will look like the one shown in Fig. 9a. It can be seen that $NHE_{pe,i}$ increases up to a maximum value and then decreases towards zero as cumulative normalized deformation increases. This is a typical behavior observed in all the cyclic responses from the finite element analysis database and also observed for the experiments conducted by Padilla-Llano et al. (2014a).

The rationale therefore is: there should be a cumulative normalized deformation CDF_0 for which $NHE_{pe,i}$ is equal to zero and beyond that point the member is unable to dissipate more energy (see Fig. 9). The value for E_T is determined as the cumulative hysteretic energy E_i corresponding to the cumulative normalized axial deformation CDF_0. Values for E_T were estimated for all members in the finite element analysis database and used to obtain the expression in Eq. 1 (see Fig 7). Note that E_T increases rapidly to infinite as slenderness λ_ℓ becomes smaller, therefore a maximum limit for the total energy dissipation capacity is proposed ($E_T \leq 113.2 P_y\delta_y$) for the members with fully effective cross-sections (i.e., $\lambda_\ell \leq 0.689$). This limit is currently set somewhat arbitrary but further work is being conducted to establish this limit based on mechanics and maximum strength principles.

$$\frac{E_T}{P_y\delta_y} = \begin{cases} 113.2 & ,\lambda_\ell \leq 0.749 \\ 64.99\lambda_\ell^{-1.489} & ,\lambda_\ell > 0.749 \end{cases} \tag{1}$$

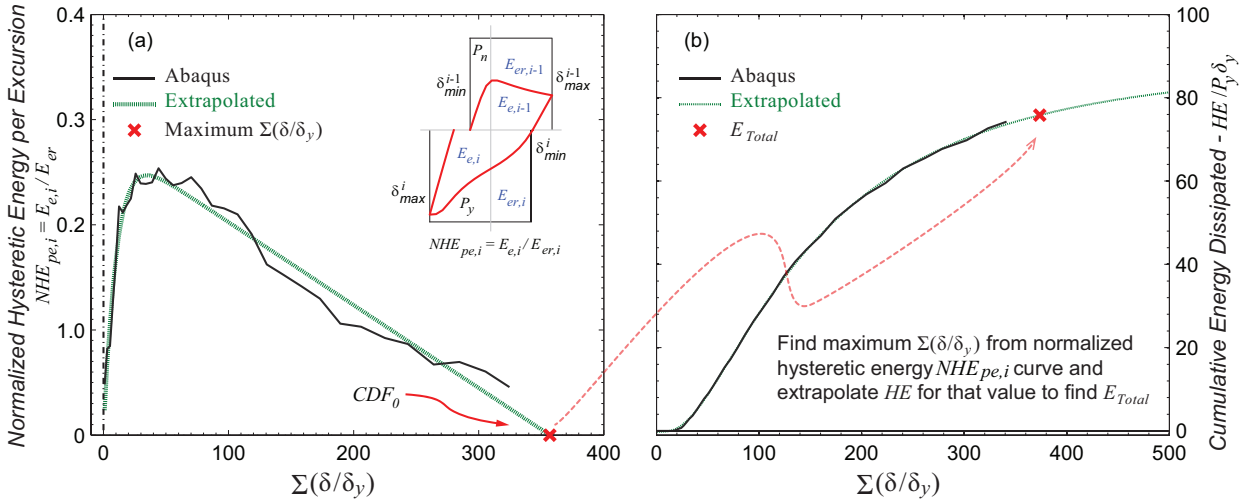

Figure 11: The total energy dissipation capacity E_T is obtained as the cumulative energy dissipated corresponding to a cumulative normalized deformation CDF_0. The cumulative deformation CDF_0 is the value where the normalized hysteretic energy per excursion $NHE_{pe,i}$ vanishes.

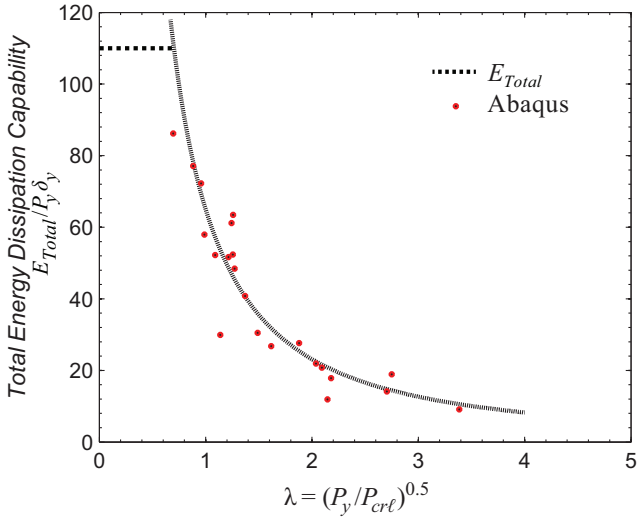

Figure 12: Total energy dissipation capability as a function of the cross-section slenderness

In *Pinching4*, E_T is expressed as a factor γ_E times the maximum between the areas below the monotonic backbone curves in tension and compression. Thus, in the case of the model described in this paper $\gamma_E = E_T / A_{BBT}$, where $A_{BBT} = 9.4 P_y \delta_y$ is the area below the tension backbone. Next section presents an example showing the strategy to model axial members experiencing local buckling deformations using the expressions previously derived.

5. Simulating the Axial Cyclic Response In Steel Columns Including Local Buckling

The two modeling approaches, *nonlinear springs* and the *nonlinear beam-column* element illustrated in Fig.3 are used to simulate the response of CFS axial members experiencing local buckling tested by Padilla-Llano et al. (2014). The spring model is implemented using rigid beam elements connected to *zeroLength* elements in OpenSees that is located at the loaded end as shown in Fig. 13b. The nonlinear beam-column model is implemented using *dispBeamColumn* elements from OpenSees connected between the two end nodes (see Fig. 13b). The parameters are derived using the expressions in Table 1-4.

The results using both modeling approaches show almost identical responses (see Fig. 13a) but underestimate the energy dissipated when compared to the experimental response (see Fig. 13b). The differences in energy and load deformation response between the models and the experimental response steams from the way *Pinching4* is implemented. The unloading-reloading from tension excursions to compression is restricted in *Pinching4* to be always monotonically increasing which prevents the models from capturing well the behavior during reloading in compression. This restriction evidently reflects in the amount of energy dissipated as well. The authors are focusing efforts to provide a hysteretic cross-section behavior model for the nonlinear-beam column that overcomes some of the issues of using *Pinching4* in modeling the axial cyclic behavior in steel columns.

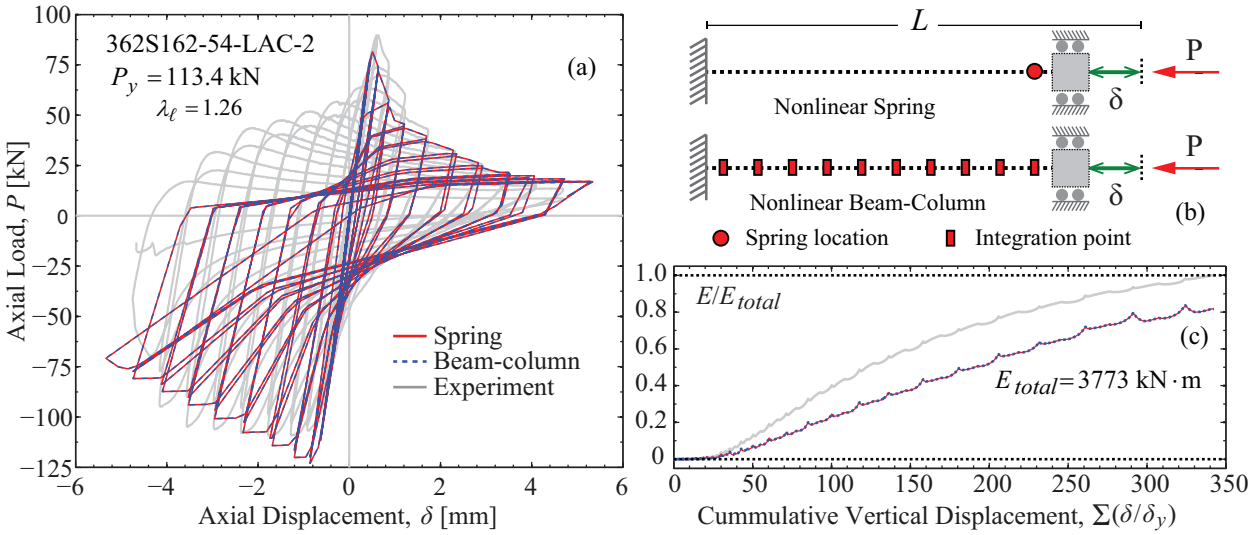

Figure 13. Simulated and experimental response (a); spring and beam-column models (b); energy dissipated (c).

6. Conclusions

This paper introduced a nonlinear model for simulating steel columns including the effects of local buckling deformations in the behavior and hysteretic energy dissipation. Model parameters are proposed in a generalized form as function of the member cross-sectional slenderness λ_ℓ that can be input directly into *Pinching4* in OpenSees. Simulation of a member axial cyclic behavior can be achieved using two presented approaches, one that considers a nonlinear spring with lumped hysteretic behavior, and a second approach that models the hysteretic behavior at the cross-section level through the use of a nonlinear beam-column element.

Both, the nonlinear spring and the nonlinear-beam column approaches supported by the hysteretic behavior model can capture the axial member cyclic response reasonably efficiently. However, spring models can present disadvantages such as displacement compatibility and difficulty when adapting the model to different loading configurations such as non-uniform axial loading, or axial loading combined with bending. In this regard, the distributed nonlinear behavior approach allows flexible modeling of steel members subjected to different axial loading conditions, e.g. the non-uniform axial load condition resulting from the contributions of individual fasteners attached to a chord stud in a CFS shear wall, among others. The authors continue working on the generalization of the parameters defining the hysteretic cross-section behavior model for the nonlinear beam-column approach addressing the issues that steam from using the current implementation of *Pinching4*.

The proposed methodology is established for thin-walled cold-formed steel members, however the *Pinching4* parameters are posed generally as a function of local buckling slenderness and could be extended to hot-rolled steel members and cross-sections with future validation.

Acknowledgments

The authors are grateful to the American Iron and Steel Institute (AISI) for funding this research and to the AISI Project Monitoring Task Group especially Bonnie Manley, Ben Schafer, Jay Larson, Colin Rogers, and Steve Tipping.

References

ABAQUS (2013). *ABAQUS Documentation v6.13*, Dassault Systèmes Simulia Corp., Providence, RI, USA.

AISI-S100-07 (2007b). *North American Specification for the Design of Cold-Formed Steel Structural Members*. American Iron and Steel Institute, Washington, D.C. ANSI/AISI-S100-07.

Lowes, L., Mitra, N., Altoontash, A., (2004). *A beam-column joint model for simulating the earthquake response of reinforced concrete frames*, PEER Report 2003/10, Pacific Earthquake Engineering Research Center.

Mazzoni, S., McKenna, F., Scott, M.H., Fenves, G.L., (2009). *Open System for Earthquake Engineering Simulation User Command-Language Manual*, OpenSees Version 2.0, Berkeley, California.

Padilla-Llano, D., Eatherton, M., Moen, C., (2013a), "Axial hysteretic modeling of cold-formed steel members for computationally efficient seismic simulation." *Structures Congress 2013*, doi: 10.1061/9780784412848.084 948-959.

Padilla-Llano, D., Moen, C., Eatherton, M., (2013b), *Energy dissipation of thin-walled cold-formed steel members*. Virginia Polytechnic Institute and State University Research Report No. CE/VPI-ST-13/06, Blacksburg, VA.

Padilla-Llano, D., Moen, C., Eatherton, M., (2014a). "Cyclic axial response and energy dissipation of cold-formed steel framing members." *Thin-Walled Structures*, vol. 78, 95-107.

Padilla-Llano, D., Moen, C., Eatherton, M., (2014b). "Local buckling hysteretic nonlinear models for cold-formed steel axial members." *Proceedings of the 22nd International Specialty Conference on Cold-Formed Steel Axial Members*, St. Louis, Missouri. 919-929.

SSMA (2011), Steel Stud Manufacturers Association, Product Technical Information, ICBO ER-4943P, <http://www.ssma.com>, (December 15, 2011).

Zeinoddini V., Schafer B., (2012), "Simulation of geometric imperfections in cold-formed steel members using spectral representation approach." *Thin-Walled Structures*; vol. 60, 105-17.